PARAMETRIC TREND STUDY DURING STABILITY ANALYSIS OF A TETHERED AEROSTAT

Rakesh Kumar, Shashank Srivastava and A.K. Ghosh
Indian Institute of Technology Kanpur, Kanpur-208 016, India
Emails : rakpec@iitk.ac.in; shashank.iet22@gmail.com; akg@iitk.ac.in

Balraj Gupta and Ajit Kumar
Aerial Delivery Research and Development Establishment (ADRDE),
Station Road, Post Box No. 51, Agra Cant, Agra - 282 001, India
Emails : directoradrde@dataone.in; ajit.kpc@gmail.com

Abstract

The paper presents the longitudinal and lateral stability analysis of an aerostat tethered in a steady wind. The parametric trend study showing the effect of variation of different parameters on longitudinal stability boundaries of an aerostat has also been presented. In contrast with the conventional airplane, the equations of motion for the tethered aerostat included buoyancy forces, apparent mass terms and static forces resulting from the tether cable. The analysis consisted of mathematical modeling and its use to compute the stability characteristics for the longitudinal and lateral cases followed by the parametric trend study carried out by varying the dimensional, aerodynamic and other parameters of the aerostat for the longitudinal case. Graphical results show that the aerostat is stable for longitudinal as well as lateral case. The parametric trend study presented, thereafter, suggested that the judicious and feasible choice of various aerostat parameters could be utilized to design a new aerostat that can remain stable for wide range of wind velocities.

Keywords*: Tethered aerostat, Stability boundaries*

Nomenclature

a	= Distance along balloon centre line from nose to reference point, m
A	= Aspect Ratio
b	= Span (planform) of the horizontal tail, m
B	= Buoyancy force, N
$\bar{c}$, c_t , c_r	= Mean, tip and root aerodynamic chords of tail, m
C_{Dc}	= Tether cable drag coefficient
C_D, C_L, C_Y	= Drag, lift and side force coefficients
C_l, C_m, C_n	= Rolling, pitching and yawing moment coefficients
d_c	= Tether cable diameter, m
D_{max}, L	= Maximum diameter and length of the aerostat, m
F_X, F_Y, F_Z	= External forces acting on balloon parallel to x, y and z axes respectively, N
h_{br} or H_{br}	= Component of distance from RP to COB, positive for COB below RP, m
h_{cg} or H_{cg}	= Component of distance from RP to COM of balloon, positive for COM below RP, m
h_{sr} or H_{sr}	= Component of distance from RP to COM of balloon structure, positive for COM below RP, m
I_x, I_y, I_z	= Rolling, pitching and yawing moments of inertia respectively about balloon COM, kg-m^2
I_{xy}, I_{xz}, I_{yz}	= Products of inertia in the XY, XZ and YZ plane respectively, kg-m^2
k_{xx}, k_{yy}, k_{zz}	= Tether force per unit displacement in x, y and z axis resp. at BCP, N/m

Paper Code : V63 N2/723-2011. Manuscript received on 19 Jul 2010. Reviewed and accepted as a Full Length Contributed Paper on 17 Feb 2011

k_{xz}, k_{zx} = Tether x-force per unit of z-displacement at BCP and vice versa, N/m

$k_{x\theta}$, $k_{z\theta}$ = Tether x and y-force per unit of pitch displacement respectively, N/rad

$k_{y\varphi}$, $k_{y\psi}$ = Tether y-force per unit of roll and yaw displacement respectively, N/rad

$k_{\theta x}$, $k_{\theta z}$ = Tether pitching moment per unit of x and y-displacement resp., N-m/m

$k_{\theta\theta}$, $k_{\varphi\varphi}$, $k_{\psi\psi}$ = Total tether pitch, roll and yaw moment per unit of pitch, roll and yaw displacement respectively about COM, N-m/rad

$k_{\theta\theta D}$, $k_{\theta\theta T}$ = $K_{\theta\theta}$ due to displacement and rotation of balloon relative to steady tension vector at BCP, N-m/rad

$k_{\varphi y}$, $k_{\psi y}$ = Tether rolling and yawing moment per unit of y-displacement, N-m/m

$k_{\varphi\psi}$, $k_{\psi\varphi}$ = Tether rolling moment/unit of yaw displacement and vice versa, N-m/rad

l = Tether cable length, m

l_{br} or L_{br} = Component of distance from RP to COB, positive for COB forward of RP, m

l_{cg} or L_{cg} = Component of distance from RP to COM of balloon, positive for COM forward of RP, m

l_{sr} or L_{sr} = Component of distance from RP to COM of balloon structure, positive for COM aft of RP, m

l_{tr} or L_{tr} = Component of distance from RP to BCP, positive for BCP forward of RP, m

L_{PHT}, L_{PVT} = Distance of CG from MAC of PHT and PVT of balloon, m

L_{VT}, L_{PVT} = Vertical distance of CG from MAC of VT and PVT of balloon, m

m_a = Apparent mass of air associated with accelerations of balloon, kg

m_g = Mass of inflation gas, kg

m_s = Balloon structural mass (including bridle, test instruments and payload), kg

m_T = Combined mass of balloon structure and inflation gas, $m_g + m_s$, kg

M_x, M_y, M_z = Rolling, pitching and yawing moment about X, Y and Z-axes resp., Nm

n = Cable drag per unit length for cable normal to the wind, N/m

p, q, r = Perturbed roll, pitch and yaw rates about X, Y and Z-axes resp., rad/s

S_{ref}, $S_{exposed}$ = Reference area ($\pi D_{max}^2/4$) and exposed planform area of aerostat, m^2

t_{tr} or T_{tr} = Component of distance from RP to BCP, positive for BCP below RP, m

t = Time in seconds

T, T_0, T_l = Tether cable tension, tension at lower and upper ends respectively, N

u, v, w = Perturbation velocities of balloon COM along X, Y and Z-axes resp., m/s

V_∞ = Steady wind velocity, m/s

Vn = Component of wind velocity normal to cable, $V_\infty \sin\gamma$, m/s

W_s = Structural weight of balloon (including bridle, payload and test instr.), N

w_c = Tether cable weight per unit length, N/m

x_t, z_t = Distance parallel to X and Z-axis from RP to COM, positive for COM forward and below RP respectively

x_1, z_1 = Coordinates of balloon COM with respect to tether cable anchor point, m

α = Perturbation angle of attack, rad

β = Angle of sideslip, rad

ε, σ = Downwash and sidewash angles, rad

Λ = Tail sweep angle, rad

γ_0, γ_l = Angles between horizontal and tether cable at lower and upper ends resp., rad

ε = Angle between principal X-axis of balloon and stability axis, rad

η = Real part of characteristic root of stab. equations, damping parameter, 1/s

φ, θ, ψ = Roll, pitch and yaw angles respectively, rad

λ = Characteristic root of stability equations ($\eta \pm i\omega$) and taper ratio

ρ = Atmospheric density, kg/m^3

ω = Imaginary part of characteristic root of stab. equations, frequency, rad/s

Subscripts

A, B, C, G = Aerodynamic, buoyancy, tether-cable and gravity force terms respectively

t = Equilibrium trim condition

0, 1 = Lower and upper end of tether cable

α , β , $\dot{\alpha}$, $\dot{\beta}$ = With respect to α , β , $\dot{\alpha}\,\bar{c}/2\,V_\infty$ and $\dot{\beta}\,\bar{c}/2\,V_\infty$ respectively

p, q, r = With respect to $p\,\bar{c}/2\,V_\infty$, $q\,\bar{c}/2\,V_\infty$ and $r\,\bar{c}/2\,V_\infty$ respectively

Abbreviations

BCP, RP = Bridle Confluence Point and Reference Point

CG, COB = Center of gravity and center of Buoyancy

COM, SCM = Balloon centre of mass and balloon structural centre of mass

VT, PVT, PHT = Vertical, projected vertical and projected horizontal tail

MAC = Mean Aerodynamic Chord

Introduction

The operations of a tethered balloon such as supporting antennas or providing an aerial platform are often impaired by the occurrence of dynamic instabilities, especially during the strong wind conditions. This paper presents a systematic approach for the stability analysis of an aerostat (Fig.1) tethered from an earth-fixed anchor point and flying in steady wind conditions. Commendable and extensive work on initial sizing, design methodology, fabrication and dynamic stability analysis of aerostats has been done by Pant et. al.[1-5]. The work on initial sizing and conceptual design has been reported by Gupta et. al.[1] and Raina et. al.[2]. Rajani et. al.[3-4] have done commendable work on dynamic stability of aerostats. The most of the work reported in this paper is based on the reports available on stability analysis and trend study of tethered aerostat [6-10]. The presented work consisted of the mathematical modeling [8,18,19] of the considered tethered aerostat, computation of the roots of characteristic equation using the mathematical model and the study of the influence of dimensional, aerodynamic and other configuration related parameters on the longitudinal stability boundaries of the considered aerostat for a range of steady wind speeds. The parametric trend study carried out neglected downwash and sidewash effects. Also, the contributions in the area of stability analysis of aerostat [11-13] and tether cable stability and dynamics [14-16] have been reported earlier.

The reported work in the section - Mathermatical Modeling of a Tethered Aerostat, describes the complete mathematical modeling which includes aerodynamic modeling, tether-cable, buoyant and gravity forces and moments. In section - Estimation of the Stability Characteristics, illustrates the steps followed for the computation of the stability characteristics along with required mathematical formulation. The stability analysis (Longitudinal and Lateral) and parameter trend study (Longitudinal) by varying the different parameters for a range of speed showing the effect on stability boundaries has been presented in section - Stability Analysis and Longititudinal Trend Study. Finally, the concluding remarks have been summarized in the conclusion section, suggesting that a judicious choice of the parameters based on trend study analysis can eliminate or greatly reduce the instabilities encountered during the strong wind conditions.

Mathematical Modeling of a Tethered Aerostat

A systematic approach for the stability analysis of an aerostat shown in Fig.1 has been followed. The stability analysis was carried out under steady wind conditions for an aerostat tethered from an earth-fixed anchor point.

Figure 2 presents the geometrical parameters and various forces and moments acting on tethered aerostat. The use of theoretical formulations [17] based on considered aerostat configuration was made for the calculation of stability derivatives which were used during the mathematical modeling to carry out the stability analysis.

Figure 3 shows the coordinate system along with forces and moments used for the derivation of equations of motion of the tethered aerostat. Tether cable forces at the lower and upper end along with related angles have also been shown in Fig.3.

Table-1 presents the geometric, mass, inertia and aerodynamic characteristics of the considered aerostat used to carry out the stability analysis. Some dimensional parameters were given while the others were calculated for the

Table-1 : Characteristics of the Considered Aerostat

Parameter (Units)	Value	Parameter (Units)	Value	Parameter (Units)	Value
L_{tr} (m)	5.98	ρ_a (kg – m^{-3})	1.09	b_{VT} (m)	8.1415
T_{tr} (m)	10.9	ρ_{he} (kg – m^{-3})	0.1759	b_{PVT} (m)	5.7572
$L_{cg\ (m)}$	-1.92	m_T (kg)	1406	b_{PHT} (m)	11.5145
H_{cg} (m)	0.68	m_{he} (kg)	355.85	S_{VT} (m^2)	44.729
L_{br} (m)	0.31	m_s (kg)	1050.15	S_{PVT} (m^2)	31.63
H_{br} (m)	0.0	$m_{x\ ,\ a}$ (kg)	488.25	S_{PHT} (m^2)	63.26
L_{sr} (m)	-3.6	$m_{y,\ a}$ (kg)	2283.6	S_{ref} (m^2)	96.769
H_{sr} (m)	2.4	$m_{z\ ,\ a}$ (kg)	2283.6	A_{VT}	1.482
l (m)	1000	I_{xx} (kg – m^{-3})	15081.44	A_{PVT}	1.048
d_c (m)	0.017	I_{yy} (kg – m^{-3})	15081.44	A_{PHT}	2.096
D_{max} (m)	11.1	I_{zz} (kg – m^{-3})	15081.44	L_{VT} (m)	4.2387
L (m)	33.85	B (N)	18354.51	L_{PVT} (m)	1.4795
c_t (m)	3.144	w_c (N/m)	2.943	L_{PHT} (m)	9.4407
c_r (m)	7.844	C_{Dc}	1.17		
$\bar{c}$ (m)	5.829	λ	0.4		

given configuration of the tethered-aerostat based on the theoretical formulations [17].

The motion of the tethered aerostat consists of small perturbations about steady flight reference conditions. A linearized analysis similar to that of a rigid airplane has been used during the mathematical modeling while taking into account the following considerations.

- The equations of motion are referred to the centre of mass of the balloon.
- The balloon is symmetric laterally and has yaw, roll and side slip angles equal to zero in the reference steady-state trimmed condition (ψ_t , φ_t , $\beta_t = 0$).
- Balloon and bridle form a rigid system.
- The tether cable is flexible, but inextensible and contributes static forces at the bridle confluence point (BCP).
- The cable weight and drag normal to the cable are needed only for determining the static cable forces, equilibrium shape of the cable and the cable derivatives.
- The longitudinal and lateral equations of motion are uncoupled.

Four different sources of external forces and moments such as aerodynamic, buoyant, tether cable and gravity act on a tethered aerostat. Therefore, the equations of motion of a tethered aerostat can be written as [8]

$$F_{X\ ,\ A} + F_{X,\ C} + F_{X\ ,\ B} + F_{X\ ,\ G} = m_{x\ ,\ o}\ \ddot{x}_e \quad (1a)$$

$$F_{Y,\ A} + F_{Y,\ C} + F_{Y,\ B} + F_{Y,\ G} = m_{y,o}\ \ddot{y}_e \quad (1b)$$

$$F_{Z,\ A} + F_{Z,\ C} + F_{Z,\ B} + F_{Z,\ G} = m_{z,\ o}\ \ddot{z}_e \quad (1c)$$

$$M_{X,\ A} + M_{X,\ C} + M_{X,\ B} + M_{X,\ G} = I_x\ \ddot{\varphi} - I_{xz}\ \ddot{\psi} \quad (1d)$$

$$M_{Y,\ A} + M_{Y,\ C} + M_{Y,\ B} + M_{Y,\ G} = I_y\ \ddot{\theta} \quad (1e)$$

$$M_{Z,\ A} + M_{Z,\ C} + M_{Z,\ B} + M_{Z,\ G} = -I_{xz}\ \ddot{\varphi} + I_z\ \ddot{\psi} \quad (1f)$$

The terms $m_{x,o}$, $m_{y,o}$ and $m_{z,o}$ are total aerostat masses in x, y and z directions respectively and can be expressed as

$$m_{x,o} = m_s + m_g + m_{a1} \tag{2a}$$

$$m_{y,o} = m_s + m_g + m_{a2} \tag{2b}$$

$$m_{z,o} = m_s + m_g + m_{a3} \tag{2c}$$

The terms m_s, and m_g are the structural mass of aerostat and mass of the gas inside the aerostat. The terms m_{a1}, m_{a2} and m_{a3} are apparent masses associated with accelerations in x, y and z directions respectively. The apparent masses which depend upon the equilibrium trim angle of attack (α_t) are given by the following equations.

$$m_{a1} = m_{x,a} \cos^2 \alpha_t + m_{z,a} \sin^2 \alpha_t \tag{3a}$$

$$m_{a2} = m_{y,a} \tag{3b}$$

$$m_{a3} = m_{x,a} \sin^2 \alpha_t + m_{z,a} \cos^2 \alpha_t \tag{3c}$$

The terms $m_{x,a}$, $m_{y,a}$ and $m_{z,a}$ are the apparent masses of the balloon accelerating along the X_b, Y_b and Z_b axes.

The mass moments of inertia which depend upon the orientation of the balloon are expressed by the following equations.

$$I_x = I_{xx} \cos^2 \varepsilon + I_{zz} \sin^2 \varepsilon \tag{4a}$$

$$I_y = I_{yy} \tag{4b}$$

$$I_z = I_{zz} \sin^2 \varepsilon + I_{zz} \cos^2 \varepsilon \tag{4c}$$

$$I_{xz} = \tfrac{1}{2} (I_{xx} - I_{zz}) \sin^2 \varepsilon \tag{4d}$$

The terms I_{xx}, I_{yy} and I_{zz} are the mass moments of inertia about the principal axes and ε is the angle between the principal X-axis and the stability X-axis. In the present analysis the X_b, Y_b and Z_b axes are considered to be principal axes; hence $\varepsilon = \alpha_t$.

Aerodynamic Forces and Moments

The aerodynamic forces and moments at trim conditions in the non-dimensional form while neglecting the higher order perturbation terms are represented by the following relationships (8).

$$F_{X,A} = -\left[\left(\frac{\rho V_\infty S}{2}\right)(2C_D + C_{D_u})\,\dot{x}_e\right] - \left[\left(\frac{\rho V_\infty S}{2}\right)(C_{D_\alpha} - C_L)\right]\dot{z}_e - \left[\left(\frac{\rho V_\infty^2 S}{2}\right)(C_{D_\alpha} - C_L)\right]\theta - \left(\frac{\rho V_\infty^2 S}{2}\right)C_D \tag{6a}$$

$$F_{Y,A} = \left[\left(\frac{\rho S \bar{c}}{4}\right)C_{Y_{\dot\beta}}\right]\ddot{y}_e + \left(\frac{\rho V_\infty S}{2} C_{Y_\beta}\right)\dot{y}_e + \left(\frac{\rho V_\infty S \bar{c}}{4} C_{Y_p}\right)\dot{\varphi} - \left[\frac{\rho V_\infty S \bar{c}}{4}(C_{Y_{\dot\beta}} - C_{Y_p})\right]\dot{\psi} - \left(\frac{\rho V_\infty^2 S}{2} C_{Y_\beta}\right)\psi \tag{6b}$$

$$F_{Z,A} = -\left[\left(\frac{\rho V_\infty S}{2}\right)(2C_L + C_{L_u})\right]\dot{x}_e - \left[\left(\frac{\rho S \bar{c}}{4}\right)C_{L_{\dot\alpha}}\right]\ddot{z}_e - \left[\left(\frac{\rho V_\infty S}{2}\right)(C_{L_\alpha} + C_D)\right]\dot{z}_e - \left[\frac{\rho V_\infty S \bar{c}}{4}(C_{L_{\dot\alpha}} + C_{L_q})\right]\dot{\theta} - \left[\frac{\rho V_\infty^2 S}{2}(C_{L_\alpha} + C_D)\right]\theta - \frac{\rho V_\infty^2 S}{2} C_L \tag{6c}$$

$$M_{X,A} = \left[\frac{\rho S (\bar{c})^2}{4} C_{l_{\dot\beta}}\right]\ddot{y}_e + \left(\frac{\rho V_\infty S \bar{c}}{2} C_{l_\beta}\right)\dot{y}_e + \left[\frac{\rho V_\infty S (\bar{c})^2}{4} C_{l_p}\right]\dot{\varphi} - \left[\frac{\rho V_\infty S (\bar{c})^2}{4}(C_{l_{\dot\beta}} - C_{l_r})\right]\dot{\psi} - \left(\frac{\rho V_\infty^2 S \bar{c}}{2} C_{l_\beta}\right)\psi \tag{6d}$$

$$M_{Y,A} = \left[\frac{\rho V_\infty S \bar{c}}{2}(2C_m + C_{m_u})\right]\dot{x}_e + \left[\frac{\rho S (\bar{c})^2}{4} C_{m_{\dot\alpha}}\right]\ddot{z}_e$$

$$+\left(\frac{\rho V_\infty S\,\bar{c}}{2} C_{m_\alpha}\right) \dot{z}_e + \frac{\rho V_\infty S (\bar{c})^2}{4} (C_{m_{\dot{\alpha}}} + C_{m_q})\,\dot{\theta}$$

$$+\left(\frac{\rho V_\infty^2 S\,\bar{c}}{2} C_{m_\alpha}\right) \theta + \frac{\rho V_\infty^2 S\,\bar{c}}{2} C_m \qquad (6e)$$

$$M_{Z,A} = \left[\frac{\rho S (\bar{c})^2}{4} C_{n_{\dot{\beta}}}\right] \ddot{y}_e + \left(\frac{\rho V_\infty S\,\bar{c}}{2} C_{n_\beta}\right) \dot{y}_e$$

$$+\left[\frac{\rho V_\infty S (\bar{c})^2}{4} C_{n_p}\right] \dot{\varphi} - \left[\frac{\rho V_\infty S (\bar{c})^2}{4} (C_{n_{\dot{\beta}}} - C_{n_r})\right] \dot{\psi}$$

$$-\left(\frac{\rho V_\infty^2 S\,\bar{c}}{2} C_{n_\beta}\right) \psi \qquad (6f)$$

Tether-Cable Forces and Moments

The tether-cable forces and moments (8) are expressed as :

$$F_{X,C} = -k_{xx} x_e - k_{xz} z_e - (k_{x\theta} + T_1 \sin\gamma_1)\,\theta + T_1 \cos\gamma_1 \qquad (7a)$$

$$F_{Y,C} = -k_{yy} y_e + (T_1 \sin\gamma_1 - k_{y\varphi})\,\varphi - (T_1 \cos\gamma_1 + k_{y\psi})\,\psi \qquad (7b)$$

$$F_{Z,C} = -k_{zx} x_e - k_{zz} z_e + (T_1 \cos\gamma_1 + k_{z\theta})\,\theta + T_1 \sin\gamma_1 \qquad (7c)$$

$$M_{X,C} = -k_{\varphi y} y_e - (h_{k_2} T_1 \sin\gamma_1 + k_{\varphi\varphi})\,\varphi + (h_{k_2} T_1 \cos\gamma_1 - k_{\varphi\psi})\,\psi \qquad (7d)$$

$$M_{Y,C} = -k_{\theta x} x_e - k_{\theta z} z_e - k_{\theta\theta}\,\theta - h_{k_1} T_1 \sin\gamma_1 + h_{k_2} T_1 \cos\gamma_1 \qquad (7e)$$

$$M_{Z,C} = -k_{\psi y} y_e + (h_{k_1} T_1 \sin\gamma_1 + k_{\psi\varphi})\,\varphi - (h_{k_1} T_1 \cos\gamma_1 - k_{\psi\psi})\,\psi \qquad (7f)$$

where

$$h_{k_1} = (l_{tr} - l_{cg}) \cos\alpha_t + (t_{tr} - h_{cg}) \sin\alpha_t$$

$$h_{k_2} = (t_{tr} - h_{cg}) \cos\alpha_t - (l_{tr} - l_{cg}) \sin\alpha_t ,$$

$$k_{x\theta} = h_{k_2} k_{xx} - h_{k_1} k_{x2} , \quad k_{z\theta} = h_{k_2} k_{zx} - h_{k_1} k_{zz}$$

$$k_{\theta x} = h_{k_2} k_{xx} - h_{k_1} k_{zx} , \quad k_{\theta z} = h_{k_2} k_{xz} - h_{k_1} k_{zz}$$

$$k_{\theta\theta} = k_{\theta\theta_D} + k_{\theta\theta_T}$$

$$k_{\theta\theta_D} = h_{k_2}^2 k_{xx} - h_{k_2} h_{k_1} (k_{xz} + k_{zx}) + h_{k_1}^2 k_{zz} ,$$

$$k_{\theta\theta_T} = h_{k_2} (T_1 \sin\gamma_1) + h_{k_1} (T_1 \cos\gamma_1)$$

$$k_{y\varphi} = -h_{k_2} k_{yy} , \quad k_{y\psi} = h_{k_1} k_{yy} , \quad k_{\varphi y} = k_{y\varphi}$$

$$k_{\varphi\varphi} = h_{k_2}^2 k_{yy} , \quad k_{\psi\psi} = h_{k_1}^2 k_{yy}$$

$$k_{\varphi\psi} = -h_{k_1} h_{k_2} k_{yy} , \quad k_{\psi y} = k_{y\psi} , \quad k_{\psi\varphi} = k_{\varphi\psi}$$

Buoyancy Forces and Moments

The expressions for the buoyancy forces and moments about the centre of mass in the stability axis system can be expressed assuming small perturbation angles as (8) :

$$F_{X,B} = B\,\theta \qquad (8a)$$

$$F_{Y,B} = -B\varphi \qquad (8b)$$

$$F_{Z,B} = -B \qquad (8c)$$

$$M_{X,B} = -B\left[(h_{cg} - h_{br}) \cos\alpha_t + (l_{br} - l_{cg}) \sin\alpha_t\right]\varphi \qquad (8d)$$

$$M_{Y,B} = B\left[(l_{br} - l_{cg}) \cos\alpha_t - (h_{cg} - h_{br}) \sin\alpha_t\right]$$
$$- B\left[(h_{cg} - h_{br}) \cos\alpha_t + (l_{br} - l_{cg}) \sin\alpha_t\right]\theta \qquad (8e)$$

$$M_{Z,B} = -B\left[(l_{br} - l_{cg}) \cos\alpha_t - (h_{cg} - h_{br}) \sin\alpha_t\right]\varphi \qquad (8f)$$

Gravity Forces and Moments

The component due to structural weight of balloon is considered during the formulation of equations of motion for gravity forces. The effects of apparent mass and lifting gas are already included in the coefficients of the acceleration and buoyancy terms respectively.

The forces and moments due to gravity for small perturbation angles are determined by:

$$F_{X,G} = -W_s\,\theta \qquad (9a)$$

$$F_{Y,G} = -W_s \varphi \tag{9b}$$

$$F_{Z,G} = -W_s \tag{9c}$$

$$M_{X,G} = -W_s\left[(h_{sr} - h_{cg})\cos\alpha_t + (l_{sr} + l_{cg})\sin\alpha_t\right]\varphi \tag{9d}$$

$$M_{Y,G} = W_s\left[(l_{sr} + l_{cg})\cos\alpha_t - (h_{sr} - h_{cg})\sin\alpha_t\right] - W_s\left[(h_{sr} - h_{cg})\cos\alpha_t + (l_{sr} + l_{cg})\sin\alpha_t\right]\theta \tag{9e}$$

$$M_{Z,G} = -W_s\left[(l_{sr} + l_{cg})\cos\alpha_t - (h_{sr} - h_{cg})\sin\alpha_t\right]\varphi \tag{9f}$$

Estimation of the Stability Characteristics

After the mathematical modeling, the stability characteristics (roots/eigen values) of the considered aerostat can be estimated by executing the following steps:

- Calculate the trim angle of attack.
- Obtain the aerodynamic parameters dependent on trim angle of attack for the steady state trim condition.
- Calculate the value of tensions in the cable at the upper and lower ends.
- Use the value of tensions to obtain tether cable derivatives.
- Obtain the stability equations by putting the equilibrium part of the balloon's equations of motion to zero.
- Convert the above stability equations in the matrix form and obtain the roots/eigen values by using the results obtained in the steps 1 to 4.

Balloon Equations of Motion

After combining all the expressions for each of the external forces and moments (such as aerodynamic, buoyancy, cable-tether and gravity), the following resulting equations of motion (8) about the balloon COM can be obtained.

x-force :

$$m_x \ddot{x}_e + \left[\frac{\rho V_\infty S}{2}(2C_D + C_{D_u})\right]\dot{x}_e + k_{xx} x_e + \left[\frac{\rho V_\infty S}{2}(C_{D_\alpha} - C_L)\right]\dot{z}_e + k_{xz} z_e + \left[k_{x\theta} + \frac{\rho V_\infty^2 S}{2}(C_{D_\alpha} - C_L) - (B - W_s) + T_1 \sin\gamma_1\right]\theta + \frac{\rho V_\infty^2 S}{2} C_D - T_1 \cos\gamma_1 = 0 \tag{10a}$$

y-force :

$$m_y \ddot{y}_e - \left(\frac{\rho V_\infty S}{2} C_{Y_\beta}\right)\dot{y}_e + k_{yy} y_e - \left(\frac{\rho V_\infty S\,\bar{c}}{4} C_{Y_p}\right)\dot{\varphi} + \left[k_{y\varphi} - T_1 \sin\gamma_1 + B + W_s\right]\varphi + \frac{\rho V_\infty S\,\bar{c}}{4}(C_{Y_{\dot\beta}} - C_{Y_r})\dot{\psi} + \left(k_{y\psi} + T_1 \cos\gamma_1 + \frac{\rho V_\infty^2 S}{2} C_{Y_\beta}\right)\psi = 0 \tag{10b}$$

z-force :

$$m_z \ddot{z}_e + \frac{\rho V_\infty S}{2}(2C_L + C_{L_u})\dot{x}_e + k_{zx} x_e + \frac{\rho V_\infty S}{2}(C_{L_\alpha} + C_D)\dot{z}_e + k_{zz} z_e + \frac{\rho V_\infty S\,\bar{c}}{4}(C_{L_{\dot\alpha}} + C_{L_q})\dot{\theta} + \left[k_{z\theta} + \frac{\rho V_\infty^2 S}{2}(C_{L_\alpha} + C_D) - T_1 \cos\gamma_1\right]\theta + \frac{\rho V_\infty^2 S}{2} C_L + B + W_s - T_1 \sin\gamma_1 = 0 \tag{10c}$$

Rolling Moment :

$$-\left[\frac{\rho S\bar{c}^2}{4} C_{l_{\dot\beta}}\right]\ddot{y}_e - \left[\frac{\rho V_\infty S\,\bar{c}}{2} C_{l_\beta}\right]\dot{y}_e + k_{\varphi y} y_e + I_x \ddot{\varphi} - \left[\frac{\rho V_\infty S\,\bar{c}^2}{4} C_{l_p}\right]\dot{\varphi} + \left[h_{k_2} T_1 \sin\gamma_1 + k_{\varphi\varphi} + M_{s_1}\right]\varphi - I_{xz}\ddot{\psi} + \left[\frac{\rho V_\infty S\,\bar{c}^2}{4}\left(C_{l_{\dot\beta}} - C_{l_r}\right)\right]\dot{\psi} + \left(\frac{\rho V_\infty^2 S\,\bar{c}}{2} C_{l_\beta} - h_{k_2} T_1 \cos\gamma_1 + k_{\varphi\psi}\right)\psi = 0 \tag{10d}$$

Pitching Moment :

$$-\left[\frac{\rho V_\infty S \bar{c}}{2}(2C_m + C_{m_u})\right]\dot{x}_e + k_{\theta x} x_e - \left[\frac{\rho S \bar{c}^2}{4} C_{m_{\dot{\alpha}}}\right]\ddot{z}_e$$

$$-\left(\frac{\rho V_\infty S \bar{c}}{2} C_{m_\alpha}\right)\dot{z}_e + k_{\theta z} z_e + I_y \ddot{\theta} - \left[\frac{\rho V_\infty S \bar{c}^2}{4}\left(C_{m_{\dot{\alpha}}} + C_{m_q}\right)\right]\dot{\theta}$$

$$+\left(k_{\theta\theta} + M_{s_1} - \frac{\rho V_\infty^2 S \bar{c}}{2} C_{m_\alpha}\right)\theta - \frac{\rho V_\infty^2 S \bar{c}}{2} C_m + h_{k_1} T_1 \sin\gamma_1$$

$$- h_{k_2} T_1 \cos\gamma_1 - M_{s_2} = 0 \qquad (10e)$$

Yawing Moment :

$$-\left[\frac{\rho S \bar{c}^2}{4} C_{n_{\dot{\beta}}}\right]\ddot{y}_e - \left[\frac{\rho V_\infty S \bar{c}}{2} C_{n_\beta}\right]\dot{y}_e + \left(k_{\psi y}\right) y_e - \left(I_{xz}\ddot{\varphi}\right)$$

$$-\left[\frac{\rho V_\infty S \bar{c}^2}{4} C_{n_p}\right]\dot{\varphi} + \left(M_{s_2} + k_{\psi\varphi} - h_{k_1} T_1 \sin\gamma_1\right)\varphi + (I_z)\ddot{\psi}$$

$$+\left[\frac{\rho V_\infty S \bar{c}^2}{4}\left(C_{n_{\dot{\beta}}} - C_{n_r}\right)\right]\dot{\psi}$$

$$+\left(\frac{\rho V_\infty^2 S \bar{c}}{2} C_{n_\beta} + h_{k_1} T_1 \cos\gamma_1 + k_{\psi\psi}\right)\psi = 0 \qquad (10f)$$

where

$$M_{s_1} = \left[\left(l_{br} - l_{cg}\right) B + \left(l_{sr} + l_{cg}\right) W_s\right] \sin\alpha_t$$

$$+\left[\left(h_{cg} - h_{br}\right) B + \left(h_{sr} - h_{cg}\right) W_s\right] \cos\alpha_t$$

$$M_{s_2} = \left[\left(l_{br} - l_{cg}\right) B + \left(l_{sr} + l_{cg}\right) W_s\right] \cos\alpha_t$$

$$-\left[\left(h_{cg} - h_{br}\right) B + \left(h_{sr} - h_{cg}\right) W_s\right] \sin\alpha_t$$

$$m_x = m_{x,o}, \quad m_y = m_{y,o} - \frac{\rho S \bar{c}}{4} C_{Y_{\dot{\beta}}},$$

$$m_z = m_{z,o} + \frac{\rho S \bar{c}}{4} C_{L_{\dot{\alpha}}}$$

Equilibrium Trim Conditions

In the mathematical model used for calculating the stability characteristic, it is seen that all the aerodynamic parameters are dependent on the angle of attack and it is required to calculate the angle of attack at which the steady state trimmed condition for the balloon is achieved, this angle of attack is called the trim angle of attack.

The steady state trimmed conditions can be obtained by setting the perturbation quantities of Equations (10a-10c) equal to zero.

$$\frac{\rho V_\infty^2 S}{2} C_D - T_1 \cos\gamma_1 = 0 \qquad (11a)$$

$$\frac{\rho V_\infty^2 S}{2} C_L + B - W_s - T_1 \sin\gamma_1 = 0 \qquad (11b)$$

$$-\frac{\rho V_\infty^2 S \tau}{2} C_m + h_{k_1} T_1 \sin\gamma_1 - h_{k_2} T_1 \cos\gamma_1 - M_{s_2} = 0 \qquad (11c)$$

Substitute Equations (11a-11b) into Equation (11c) to eliminate the cable tension T_1 and angle γ_1 to obtain the following trim equation:

$$h_{k_1}\left(\frac{\rho V_\infty^2 S}{2} C_L + B - W_s\right) - h_{k_2}\left(\frac{\rho V_\infty^2 S}{2} C_D\right)$$

$$- \frac{\rho V_\infty^2 S}{2} C_{cm} - M_{s_2} = 0 \qquad (12)$$

Equation (12) can be solved by Newton iterations to find the equilibrium trim angle of attack (α_t) for various wind velocities, provided the aerodynamic coefficients C_L, C_D, and C_m are known functions of α_t. The calculated α_t can be used to solve the Equations (11a-11c) to find T_1 and γ_1 followed by the evaluation of α dependent stability coefficients.

Formulations for Calculation of Stability Derivatives

The expressions for the longitudinal and lateral stability coefficient/derivatives calculated in the previous step are based on the theoretical formulation corresponding to CG location. The derivatives based on the aerostat configuration have been calculated for projected horizontal

(PHT), vertical (VT) and projected vertical (PVT) tail. Lift curve slope expression given in Equation (13) uses the values of constants of the respective tail (PHT, PVT or VT).

$$C_{L_{\alpha_t}} = \frac{(2\pi A)}{\left(2 + \sqrt{4 + \frac{A^2}{\eta^2}\beta^2\left(1 + \frac{\tan^2\Lambda}{\beta^2}\right)}\right)} * \frac{S_{exposed}}{S_{ref}} \tag{13}$$

where $C_{L_{\alpha_t}}$ is the lift curve slope of the tail.

Longitudinal Derivatives (PHT)

$$C_L = 0.0061 + 1.2\alpha + C_{L_{\alpha_t}}\alpha + \eta\, C_{D_c}\frac{S_p}{S_{ref}}\alpha^2,$$

$$C_{L_\alpha} = 1.2 + C_{L_{\alpha_t}} + 2\eta\, C_{D_c}\frac{S_p}{S_{ref}}\alpha$$

$$C_{L_{\dot\alpha}} = C_{L_q}\frac{d\varepsilon}{d\alpha}, \qquad C_{L_q} = 2C_{L_{\alpha_t}}\frac{L_{PHT}}{D}$$

$$C_D = 0.0396 + \frac{C_L^2}{\pi e A}, \qquad C_{D_\alpha} = 2\frac{C_L}{\pi e A}C_{L_\alpha}$$

$$C_m = -0.02 + 0.04832\,\alpha + \eta\, C_{L_{\alpha_t}}\left(1 - \frac{de}{d\alpha}\right)\frac{L_{PHT}}{D}\alpha$$

$$C_{m_\alpha} = 0.04832 + \eta\, C_{L_{\alpha_t}}\left(1 - \frac{de}{d\alpha}\right)\frac{L_{PHT}}{D}\alpha,$$

$$C_{m_q} = -2\,C_{L_{\alpha_t}}\left(\frac{L_{PHT}}{D}\right)^2$$

$$C_{m_{\dot\alpha}} = C_{m_q}\tau\frac{d\varepsilon}{d\alpha} \qquad \text{where} \quad \tau = \left(\frac{V_t}{V}\right)^2$$

Laterial Derivatives (VT)

$$C_{y_\beta} = -C_{L_{\alpha_t}}\frac{d\sigma}{d\beta}, \qquad C_{y_r} = C_{L_{\alpha_t}}\left(2\frac{L_{PHT}}{D} + \frac{\partial\sigma}{\partial r}\right),$$

$$C_{y_p} = C_{L_{\alpha_t}}\left(2\frac{L_{VT}}{D} - \frac{\partial\sigma}{\partial p}\right)$$

$$C_{l_\beta} = -C_{L_{\alpha_t}}\left(\frac{L_{VT}}{D}\right)\left(1 - \frac{d\sigma}{d\beta}\right)\left(\frac{V_F}{V}\right)^2,$$

$$C_{n_\beta} = C_{L_{\alpha_t}}\left(\frac{L_{PHT}}{D}\right)\left(1 - \frac{d\sigma}{d\beta}\right)\left(\frac{V_F}{V}\right)^2$$

$$C_{l_r} = C_{L_{\alpha_t}}\left(2\frac{L_{PHT}}{D} + \frac{\partial\sigma}{\partial r}\right)\left(\frac{L_{VT}}{D}\right),$$

$$C_{n_r} = -C_{L_{\alpha_t}}\left(2\frac{L_{PHT}}{D} + \frac{\partial\sigma}{\partial r}\right)\left(\frac{L_{PHT}}{D}\right)$$

$$C_{l_p} = -C_{L_{\alpha_t}}\left(2\frac{L_{VT}}{D} - \frac{\partial\sigma}{\partial p}\right)\left(\frac{L_{VT}}{D}\right),$$

$$C_{n_p} = C_{L_{\alpha_t}}\left(2\frac{L_{VT}}{D} - \frac{\partial\sigma}{\partial p}\right)\left(\frac{L_{PHT}}{D}\right)$$

Lateral Derivatives (PVT)

$$C_{y_\beta} = -C_{L_{\alpha_t}}\frac{d\sigma}{d\beta}, \qquad C_{y_r} = C_{L_{\alpha_t}}\left(2\frac{L_{PHT}}{D} + \frac{\partial\sigma}{\partial r}\right),$$

$$C_{y_p} = -C_{L_{\alpha_t}}\left(2\frac{L_{VT}}{D} - \frac{\partial\sigma}{\partial p}\right)$$

$$C_{l_\beta} = C_{L_{\alpha_t}}\left(\frac{L_{VT}}{D}\right)\left(1 - \frac{d\sigma}{d\beta}\right)\left(\frac{V_F}{V}\right)^2,$$

$$C_{n_\beta} = C_{L_{\alpha_t}}\left(\frac{L_{PHT}}{D}\right)\left(1 - \frac{d\sigma}{d\beta}\right)\left(\frac{V_F}{V}\right)^2$$

$$C_{l_r} = -C_{L_{\alpha_t}}\left(2\frac{L_{PHT}}{D} + \frac{\partial\sigma}{\partial r}\right)\left(\frac{L_{VT}}{D}\right),$$

$$C_{n_r} = -C_{L_{\alpha_t}}\left(2\frac{L_{PHT}}{D} + \frac{\partial\sigma}{\partial r}\right)\left(\frac{L_{PHT}}{D}\right)$$

$$C_{l_p} = -C_{L_{\alpha_t}}\left(2\frac{L_{VT}}{D} - \frac{\partial\sigma}{\partial p}\right)\left(\frac{L_{VT}}{D}\right),$$

$$C_{n_p} = -C_{L_{\alpha_t}}\left(2\frac{L_{VT}}{D} - \frac{\partial\sigma}{\partial p}\right)\left(\frac{L_{PHT}}{D}\right)$$

Lateral derivatives for complete vertical tail can be obtained by adding the corresponding derivatives of vertical tail and projected vertical tail.

Equilibrium Cable Shape

The forces acting on tether cable of length (Fig.4) are the tension, cable weight and drag normal to the cable. Drag along the cable has been neglected. The normal drag force per unit length depends on the component of wind velocity normal to the cable V_n, the drag cable coefficient C_{D_c} and cable diameter d_c and can be expressed as(8):

$$n = C_{D_c}\, d_c \frac{1}{2} \rho V_n^2 \tag{14}$$

Tension (T_1) at upper end of the cable using tension $\left[\frac{dT}{T} = -\frac{\bar{P}}{\bar{q}}\left(\frac{df}{\bar{q}+\bar{p}-f}+\frac{df}{\bar{q}+\bar{p}-f}\right)\right]$ is given by

$$T_1 = T\,\tau_1/\tau$$

where

$$\tau(\gamma) = \left(\frac{\bar{q}+\bar{p}-\cos\gamma}{\bar{q}-\bar{p}+\cos\gamma}\right)^{\frac{\bar{p}}{\bar{q}}},\ \bar{p}=\frac{w_c}{2n},\ \bar{q}=\sqrt{1+(\bar{p})^2},\ f=\cos\gamma \tag{15}$$

For the known parameters such as

$$l\left(dl = \left(\frac{T_1}{n\,\tau_1}\right)\frac{\tau}{(\sin^2\gamma+2\bar{p}\cos\gamma)}\,d\gamma\right)\ n,\ W_c, T_1 \text{ and } \gamma_1,$$

the following expressions can be used to determine the coordinates $\tilde{x}$ and $\tilde{z}_1$ at the upper end and T_0 and γ_0 at the lower end.

$$\bar{\lambda}_0 = \bar{\lambda}_1 - \frac{n\,\tau_1\,l}{T_1} \quad \text{and} \quad T_0 = T_1\,\tau_0/\tau_1 \tag{16}$$

$$\tilde{x}_1 = \frac{T_1}{n\,\tau_1}\int_{\gamma_0}^{\gamma_1}\frac{\tau\cos\gamma}{\left(\sin^2\gamma+2\bar{p}\cos\gamma\right)}\,d\gamma$$

where

$$d\sigma = \frac{\tau\cos\gamma}{\left(\sin^2\gamma+2\bar{p}\cos\gamma\right)}\,d\gamma \tag{17}$$

$$\tilde{z}_1 = \frac{T_1-T_0}{w_c} \quad \text{where } d\tilde{z} = dl\sin\gamma = \frac{dT}{w_c} \tag{18}$$

where

$$\tilde{\lambda}(\gamma) = \int_0^{\gamma}\frac{\tau(\gamma)}{\left(\sin^2\gamma+2\bar{p}\cos\gamma\right)}d\gamma,\ \tilde{\lambda}_0 = \tilde{\lambda}(\gamma_0) \text{ and } \tilde{\lambda}_1 = \tilde{\lambda}(\gamma_1)$$

Cable Force Derivatives

Consider the cable in its equilibrium position. If the upper end is slowly displaced in the $\tilde{x}\,\tilde{z}$ - plane from its original position $(\tilde{x}_1, \tilde{z}_1)$ to a new position $(\tilde{x}_1 + d\tilde{x}, \tilde{z}_1 + d\tilde{z})$, the resultant x- and z-force increments are

$$dF_x = k_{xx}\,d\tilde{x} + k_{xz}\,d\tilde{z} \quad \text{and} \quad dF_z = k_{zx}\,d\tilde{x} + k_{zz}\,d\tilde{z} \tag{19}$$

The cable derivatives (spring constants) k_{xx}, k_{xz}, k_{zx} and k_{zz} for the longitudinal case can be expressed as(8):

$$k_{xx} = \frac{1}{\delta}\left[T_1\cos\gamma_1(\sin\gamma_1-\sin\gamma_0) + n\,(z_1 - l\sin\gamma_0)\sin^3\gamma_1\right] \tag{20a}$$

$$k_{xz} = \frac{1}{\delta}\left[T_1\cos\gamma_1(\cos\gamma_0-\cos\gamma_1) + n\,(l\cos\gamma_0 - \tilde{x}_1)\sin^3\gamma_1\right] \tag{20b}$$

$$k_{zx} = \frac{1}{\delta}\left[T_1\sin\gamma_1(\sin\gamma_1-\sin\gamma_0) - (w_c + n\sin^2\gamma_1\cos\gamma_1)(\tilde{z}_1 - l\sin\gamma_0\right] \tag{20c}$$

$$k_{zz} = \frac{1}{\delta}\left[T_1\sin\gamma_1(\cos\gamma_0-\cos\gamma_1) - (w_c + n\sin^2\gamma_1\cos\gamma_1)(l\cos\gamma_0 - \tilde{x}_1\right] \tag{20d}$$

where

$$\delta = x_1(\sin\gamma_1-\sin\gamma_0) + z_1(\cos\gamma_0-\cos\gamma_1) - l\sin(\gamma_1-\gamma_0)$$

The single lateral cable derivative determined by considering a small force dF_Y to act in the y-direction on the upper end of the cable is given by the following expression.

$$dF_Y = k_{yy}\,dy$$

where

$$k_{yy} = \frac{n\sqrt{\tau_1 (\sin^2\gamma_1 + 2\,\bar{p}\cos\gamma_1)}}{\int_{\gamma_0}^{\gamma_1}\sqrt{\frac{\tau(\gamma)}{(\sin^2\gamma + 2\,\bar{p}\cos\gamma)}}\,d\gamma} \tag{21}$$

Stability Equations

The stability equations are obtained by setting the equilibrium trim portions of the equations of motion (Equations (10a-10f)) equal to zero. The following working forms of the stability equations (8) written about the balloon centre of mass are obtained.

Longitudinal Equations of Motion

X-force :

$$m_x \ddot{x}_e + \left[\frac{\rho V_\infty S}{2}(2C_D + C_{D_u})\right]\dot{x}_e + k_{xx}\,x_e + \left[\frac{\rho V_\infty S}{2}(C_{D_\alpha} - C_L)\right]\dot{z}_e + k_{xz}\,z_e + \left[k_{x\theta} + \frac{\rho V_\infty^2 S\,C_{D_\alpha}}{2}\right]\theta = 0 \tag{22a}$$

Z-force :

$$m_z \ddot{z}_e + \frac{\rho V_\infty S}{2}(2C_L + C_{L_u})\,\dot{x}_e + k_{zx}\,x_e + \frac{\rho V_\infty S}{2}(C_{L_\alpha} + C_D)\,\dot{z}_e + k_{zz}\,z_e + \frac{\rho V_\infty S\,\bar{c}}{4}(C_{L_{\dot\alpha}} + C_{L_q})\,\dot\theta + \left(-k_{z\theta} + \frac{\rho V_\infty^2 S\,C_{L_\alpha}}{2}\right)\theta = 0 \tag{22b}$$

Pitching Moment :

$$-\left[\frac{\rho V_\infty S\,\bar{c}}{2}(2C_m + C_{m_u})\right]\dot{x}_e + k_{\theta x}\,x_e - \left[\frac{\rho S\,\bar{c}^2}{4}C_{m_{\dot\alpha}}\right]\ddot{z}_e - \left(\frac{\rho V_\infty S\,\bar{c}}{2}C_{m_\alpha}\right)\dot{z}_e + k_{\theta z}\,z_e + I_y\ddot\theta - \left[\frac{\rho V_\infty S\,\bar{c}^2}{4}\left(C_{m_{\dot\alpha}} + C_{m_q}\right)\right]\dot\theta + \left(k_{\theta\theta} + M_{s_1} - \frac{\rho V_\infty^2 S\,\bar{c}}{2}C_{m_\alpha}\right)\theta = 0 \tag{22c}$$

Lateral Equations of Motion

Y-force :

$$m_y \ddot{y}_e - \left(\frac{\rho V_\infty S}{2}C_{Y_\beta}\right)\dot{y}_e + k_{yy}\,y_e - \left(\frac{\rho V_\infty S\,\bar{c}}{4}C_{Y_p}\right)\dot\varphi + \left[k_{y\varphi} - \frac{\rho V_\infty^2 S\,C_L}{4}\right]\varphi + \frac{\rho V_\infty S\,\bar{c}}{4}(C_{Y_{\dot\beta}} - C_{Y_r})\,\dot\psi + \left(k_{y\psi} + \frac{\rho V_\infty^2 S\,(C_{Y_\beta} + C_D)}{2}\right)\psi = 0 \tag{23a}$$

Rolling Moment :

$$-\left[\frac{\rho S\,\bar{c}^2}{4}C_{l_{\dot\beta}}\right]\ddot{y}_e - \left[\frac{\rho V_\infty S\,\bar{c}}{2}C_{l_\beta}\right]\dot{y}_e + k_{\varphi y}\,y_e + I_x\ddot\varphi - \left[\frac{\rho V_\infty S\,\bar{c}^2}{4}C_{l_p}\right]\dot\varphi + \left[h_{k_2}T_1\sin\gamma_1 + k_{\varphi\varphi} + M_{s_1}\right]\varphi - I_{xz}\ddot\psi + \left[\frac{\rho V_\infty S\,\bar{c}^2}{4}\left(C_{l_{\dot\beta}} - C_{l_r}\right)\right]\dot\psi + \left(\frac{\rho V_\infty^2 S\,(\bar{c}\,C_{n_\beta} + h_{k_1}C_D)}{2} + k_{\varphi\psi}\right)\psi = 0 \tag{23b}$$

Yawing Moment :

$$-\left[\frac{\rho S\,\bar{c}^2}{4}C_{n_{\dot\beta}}\right]\ddot{y}_e - \left[\frac{\rho V_\infty S\,\bar{c}}{2}C_{n_\beta}\right]\dot{y}_e + \left(k_{\psi y}\right)y_e - \left(I_{xz}\ddot\varphi\right) - \left[\frac{\rho V_\infty S\,\bar{c}^2}{4}C_{n_p}\right]\dot\varphi + \left(M_{s_2} + k_{\psi\varphi} - h_{k_1}T_1\sin\gamma_1\right)\varphi + (I_z)\ddot\psi + \left[\frac{\rho V_\infty S\,\bar{c}^2}{4}\left(C_{n_{\dot\beta}} - C_{n_r}\right)\right]\dot\psi$$

$$+\left(\frac{\rho V_{\infty}^{2} S\,(\bar{c}\,C_{n_{\beta}} + h_{k_l}\,C_D)}{2} + k_{\psi\psi}\right)\psi = 0 \qquad (23c)$$

Using the mathematical model, the stability equations can be written in the state space form as given below:

$$\frac{dx}{dt} = Ax + Bu \qquad (24)$$

where A is the characteristic matrix and B is the input matrix. Since no control input is being used, therefore the matrix A gives the characteristics of the aerostat system.

The equation for longitudinal and lateral stability case can be expressed in the following matrix form respectively.

$$\begin{bmatrix} \dot{u} \\ \dot{w} \\ \dot{q} \\ \dot{\theta} \\ \dot{x} \\ \dot{z} \end{bmatrix} = A \begin{bmatrix} u \\ w \\ q \\ \theta \\ x \\ z \end{bmatrix} \quad \text{and} \quad \begin{bmatrix} \dot{v} \\ \dot{p} \\ \dot{r} \\ \dot{\varphi} \\ \dot{\psi} \\ \dot{y} \end{bmatrix} = A \begin{bmatrix} v \\ p \\ r \\ \varphi \\ \psi \\ y \end{bmatrix} \qquad (25)$$

The roots of characteristic equation obtained by computing stability matrix A for longitudinal and lateral case give an insight into the stability of the system.

Stability Analysis and Longitudinal Trend Study

The computed values of longitudinal frequencies (ω) and damping rates (η) for the considered aerostat have been plotted as a function of wind velocity in Figs.5(a-b) and in root locus form in Fig.5c. Figs.(5a-5b) indicate that the considered aerostat has three oscillatory modes of motion for the given range of the wind velocities. First two modes (1 and 2) represent the aerodynamic modes such as 'short period mode' and 'long period mode (Phugoid mode)' whereas the third mode represents the tether cable mode. It can be observed that the aerostat is longitudinally stable except at and below wind velocity of 2 m/s at which one of the roots becomes positive (Fig. 5b). It could also be observed (Fig. 5b) that mode 2 splits into two real non-oscillatory modes above wind velocity of 19 m/s and again merged into one at 35 m/s. The negative slope between pitching moment coefficient and angle of attack (Fig.5d) infers that the aerostat is stable longitudinally.

The computed values of lateral frequencies (ω) and damping rates (η) for the considered aerostat have been plotted as a function of wind velocity in Figs.6(a-b) and in root locus form in Fig.6c. Figs.(6a-6b) indicate that the considered aerostat has three oscillatory modes of motion for the given range of the wind velocities. Fig.6b indicates that none of the modes for the considered aerostat configuration was unstable.

Next, a parametric trend study was carried out to see the effect of variation of different dimensional and aerodynamic parameters of the considered aerostat on longitudinal stability boundaries.

The results showing the effect of different parameters on the stability boundaries for a range of speed have been presented in graphical form. Figs.(7-20) show that the aerostat is unstable below the speed of 2 m/sec and in the region bounded by the two curved/straight boundaries except Fig.13, which shows the effect of increase in tether cable length on the stability of the aerostat in terms of damping for a particular wind speed. Rest of the region (above 2 m/s) represents the stable region. The unstable region increases or decreases with increase or decrease in the values of most of the dimensional and aerodynamic parameters of the considered aerostat. Very little or negligible effect on stability boundaries was observed for some parameters.

It can be observed (Figs.7-19) that the parameters such as L_{tr}, T_{tr}, L_{br}, L_{sr}, m_{he}, B, C.G. (moment arm), a_c, w_c, C_{Dc}, C_{mo} affect the stability boundaries strongly while the parameters such as L_{cg}, H_{cg}, H_{br}, H_{sr}, $C_{L\alpha\_PHT}$ and downwash have very little or negligible effect on the stability characteristics/boundaries of the aerostat.

It can be observed that the decrease in L_{tr} (the horizontal component of distance between RP and BCP) decreases the unstable region while decrease in T_{tr} (the vertical component of distance between RP and BCP) increases the unstable region (Figs.7(a-b)). The change in horizontal (L_{cg}) or vertical (H_{cg}) component of distance from RP to COM has very little or negligible effect on the stability boundaries (Figs. 8(a-b)). Increase in the value of horizontal component of distance from RP to COB (L_{br}) and COM of structure (L_{sr}) decreases the unstable regions while the vertical components (H_{br} and H_{sr}) have negligible effect (Figs.9(a-b) and 10(a-b)). Greater the mass (m_{he}) and the buoyant force (B) of the helium gas lesser will be the unstable region (Figs.(11-12)). Fig.13 presents a plot between damping and the tether cable length for short period

mode for a wind speed of 20 m/s. It can be observed from Fig.13 that the damping keeps on increasing with increase in the tether cable length leading to increase in the longitudinal stability with increase in the tether cable length. Reduction in the cable diameter (d_c), the cable weight (w_c) and the cable drag coefficient (CDc) leads to the reduction in the unstable region (Figs.(14-16)). Increase in the horizontal tail moment arm and zero lift pitching moment coefficient reduces the unstable region (Figs.(17-18)) while the change in downwash and lift curve slope of horizontal projected tail have negligible effect on stability characteristics of the aerostat (Figs.(19-20)).

Conclusion

A stability analysis and trend study for a balloon tethered in a steady wind has been presented. Equations of motion of the considered aerostat included aerodynamic, tether-cable, buoyancy and gravity forces along with aerodynamic apparent mass and structural mass terms. After mathematical modeling, the roots of the characteristic stability equation were computed and plotted for various steady-wind conditions. It was observed from graphical presentations that the considered aerostat was stable longitudinally as well as laterally. Later on, parameter trend study was carried out to show the influence of various dimensional and aerodynamic parameters of aerostat on longitudinal stability boundaries for a wide range of steady-wind speeds. The study suggests that the judicious and feasible choice of various parameters can be utilized to design a new tethered aerostat which can remain stable for a wide range of wind speeds. The limitation of the stability analysis carried out was that the downwash and sidewash terms have been neglected. Also, the effect of ballonet and its dynamics has been neglected during the analysis.

References

1. Gupta, P. and Pant, R.S., "A Methodology for Initial Sizing and Conceptual Design Studies of an Aerostat", International Seminar on Challenges on Aviation Technology, Integration and Operations (CATIO-05), Technical. Sessions of 57th Annual General Meeting of Aeronautical Society of India, December, 2005.

2. Raina, A.A., Bhandari, K.M. and Pant, R.S., "Conceptual Design of a High Altitude Aerostat for Study of Snow Patterns", Proceedings of International Symposium on Snow and Avalanches (ISSA-09), SASE, Manali, India, April 6-10, 2009.

3. Rajani, A., Pant, R.S. and Sudhakar, K., "Dynamic Stability Analysis of a Tethered Aerostat", Proceedings of 18th AIAA Lighter-Than-Air System Technology Conference, Seattle, Washington, USA, May 4-7, 2009.

4. Rajani, A., Pant, R.S. and Sudhakar, K., "Dynamic Stability Analysis of a Tethered Aerostat", Journal of Aircraft, Vol. 47, No. 5, September-October, 2010.

5. Gawande, V.N., Bilaye, P., Gawale, A.C., Pant, R.S. and Desai, U.B., "Design and Fabrication of an Aerostat for Wireless Communication in Remote Areas", System Technology Conference, Belfast, Northern Ireland, UK, September, 2007.

6. Redd, L.T., Benett, R.M. and Bland, S.R., "Analytical and Experimental Investigation of Stability Parameters for a Balloon Tethered in Wind", 7th AF Cambridge Research Laboratories Scientific Balloon Symposium (Portsmouth, N.H.), September, 1972.

7. Redd, L.T., Benett, R.M. and Bland, S.R., "Experimental and Analytical Determination of Stability Parameters for a Balloon Tethered in Wind", Numeric Value TD D-2021, 1973.

8. Redd, L.T., Benett, R.M. and Bland, S.R., "Stability Analysis and Trend Study of a Balloon Tethered in Wind, with Comparisons", NASA TN D-7272, October, 1973.

9. Srivastava Shashank., "Stability Analysis and Parameter Trend Study of Single Tether Aerostats", M.Tech Thesis, Department of Aerospace Engineerring, Indian Institute of Technology, Kanpur, April, 2009.

10. Khouri, G.A. and Gillett, J.D., "Airship Technology", Cambridge University Press, UK, 1999.

11. Delaurier, J.D., "A Stability Analysis for Tethered Aerodynamically Shaped Balloons", Journal of Aircraft, Vol. 9, No. 9, pp. 646-651, September, 1972.

12. Lambert, C. and Nahon, M., "Stability Analysis of a Tethered Aerostat", Journal of Aircraft, Vol.40, No.4, July-August, 2003, .

13. Li, Y. and Nahon, M., "Modeling and Simulation of Airship Dynamics", Journal of Guidance, Control

and Dynamics, Vol.30, No.6, November.-December, 2007.

14. Neumark, S., "Equilibrium Configurations of Flying Cables of Captive Balloons and Cable Derivatives for Stability Calculations", R and M No.3333, Brit., A.R.C, 1963.

15. Delaurier, J.D., "A First Order Theory for Predicting the Stability of Cable Towed and Tethered Bodies Where the Cable has a General Curvature and Tension Variation", VKI-TN-68, Von Karman Institute of Fluid Dynamics, December, 1970.

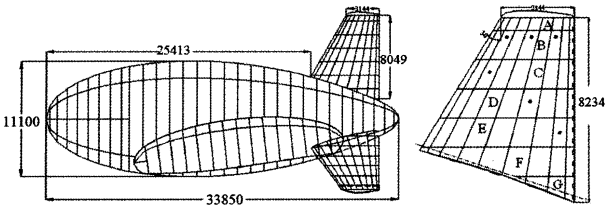

Fig.1 Dimensions of the Aerostat and Fin (mm)

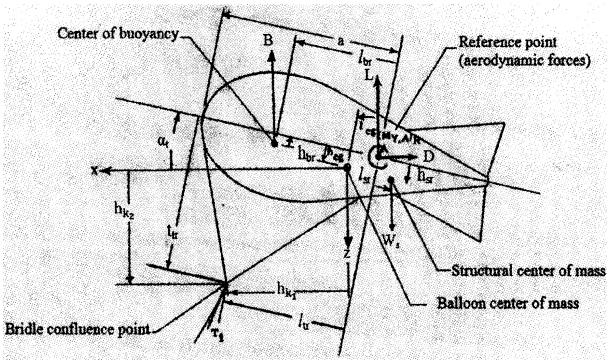

Fig.2 Geometry of the Balloon System [8]

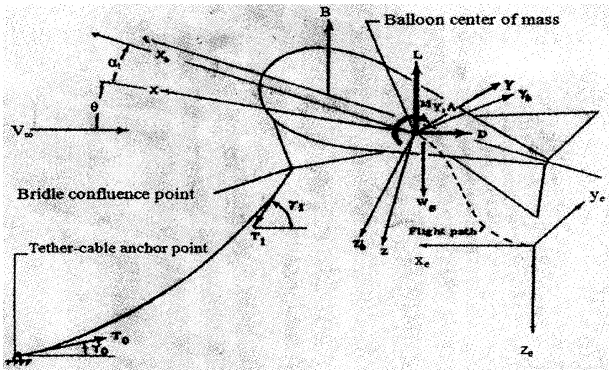

Fig.3 Coordinate System and Forces Acting on Tethered-Aerostate [8]

16. Delaurier, J.D., "A Stability Analysis of Cable-body System Totally Immersed in Fluid Stream", Numeric Value CR-2021, 1972.

17. Raymer, D.P., "Aircraft Design: A Conceptual Approach", 4th Ed. AIAA Education Series, New York, NY, 2006.

18. Etkin, B. and Lloyd, D.R., "Dynamics of Flight: Stability and Control", 3rd Ed. John Wiley and Sons Inc., 1996.

19. Nelson, R.C., "Flight Stability and Automatic Control", 2nd Ed. McGraw-Hill, 1998.

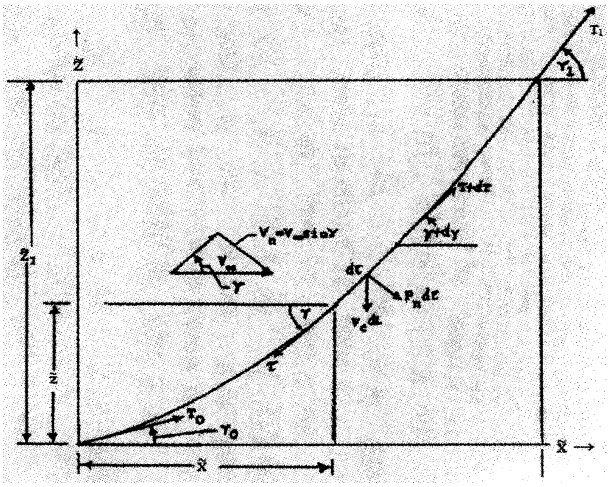

Fig.4 Forces Acting on the Tether Cable [8]

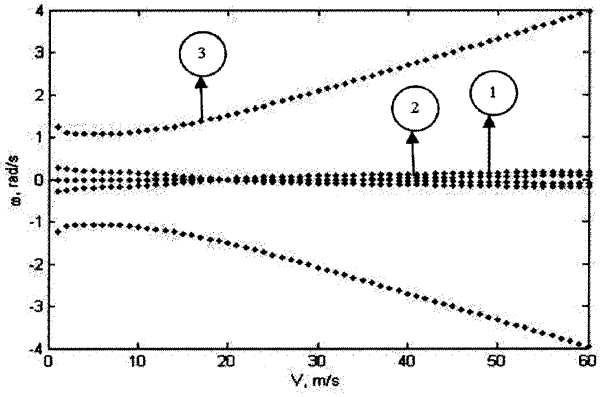

Fig.5a Variation of ω with V for Longitudinal Case

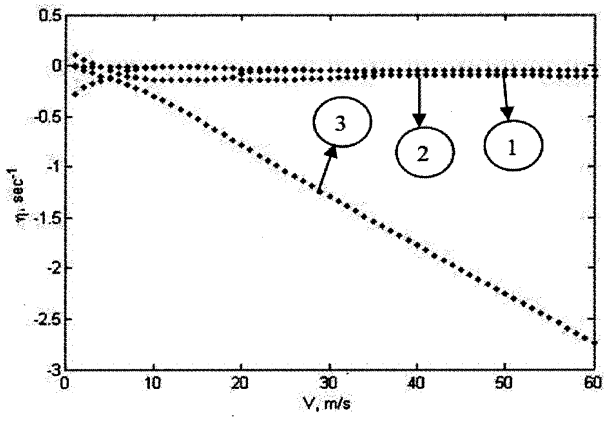

Fig.5b Variation of η with V for Longitudinal Case

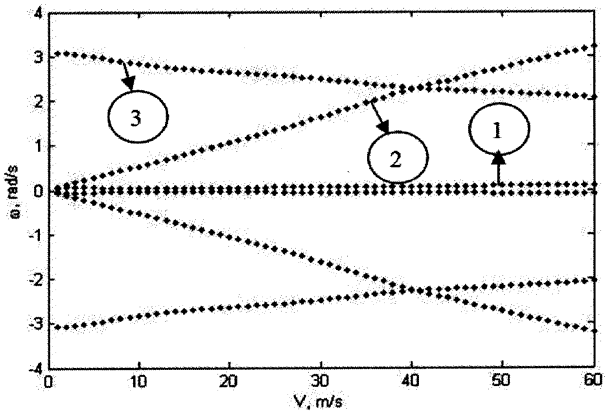

Fig.6a Variation of ω with V for Lateral Case

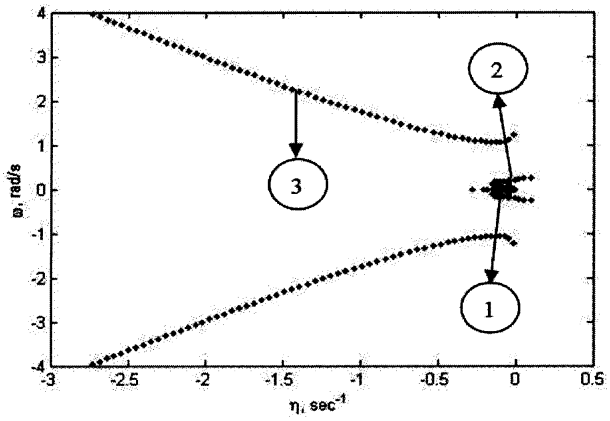

Fig.5c ω Versus η (Root-Locus Plot for Longitudinal Case)

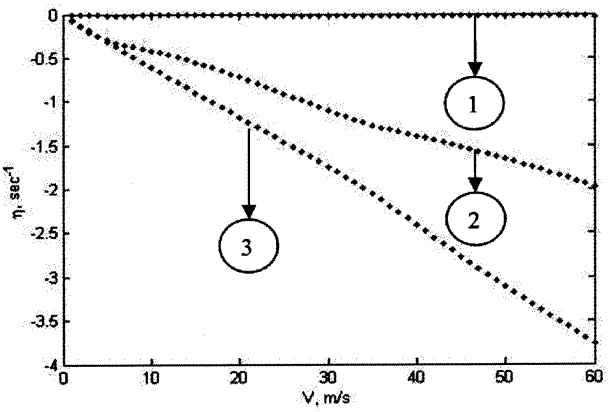

Fig.6b Variation of η with V for Lateral Case

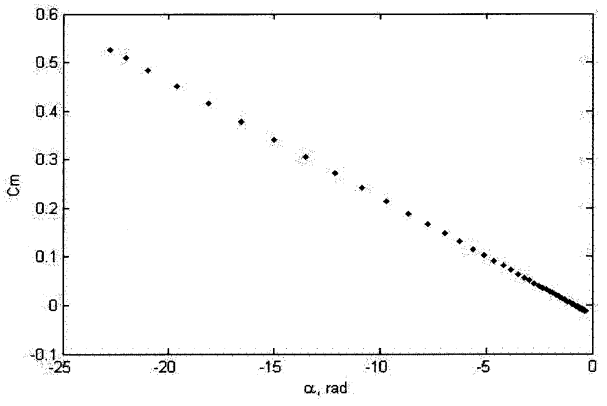

Fig.5d C_m Versus α for Longitudinal Case

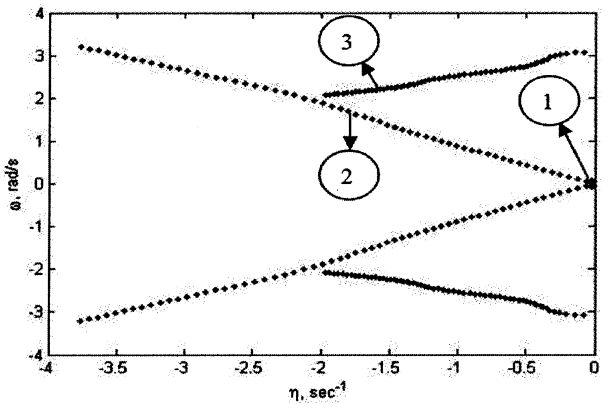

Fig.6c ω Versus η (Root-Locus Plot for Lateral Case)

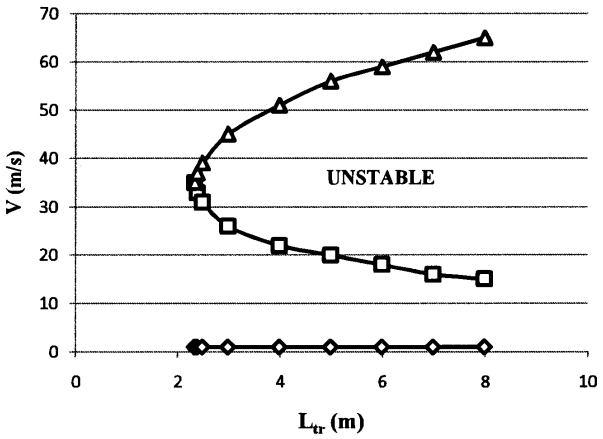

Fig. 7a Effect of L_{tr} (m) on Longitudinal Stability Boundary

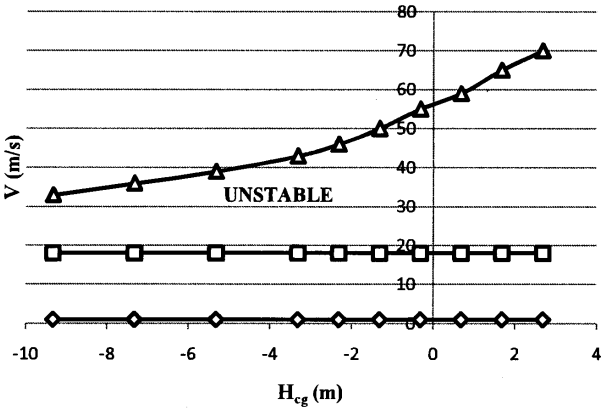

Fig.8b Effect of H_{cg} (m) on Longitudinal Stability Boundary

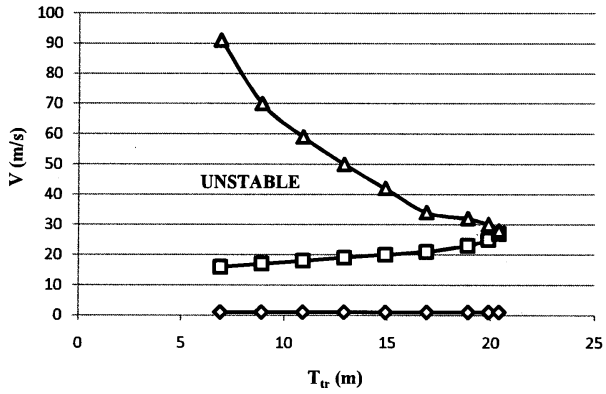

Fig.7b Effect of T_{tr} (m) on Longitudinal Stability Boundary

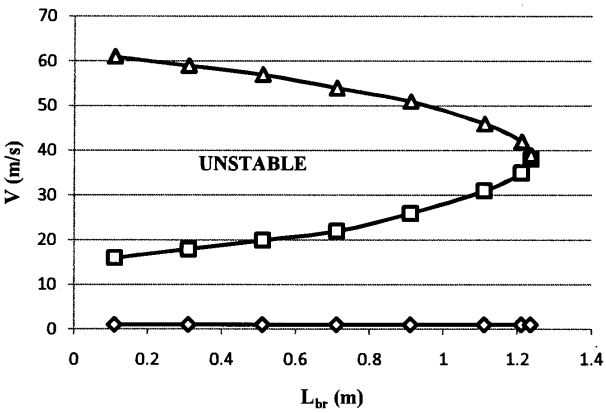

Fig.9a Effect of L_{br} (m) on Longitudinal Stability Boundary

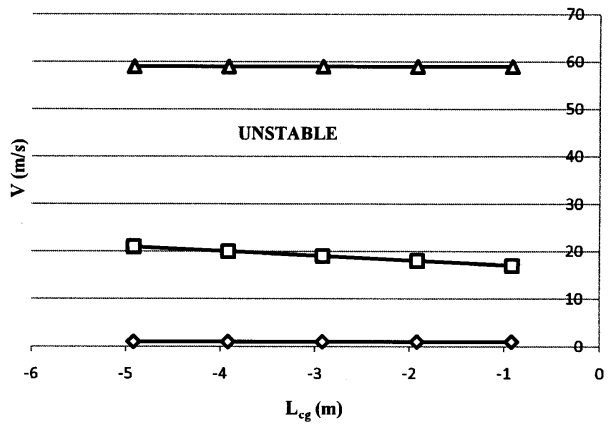

Fig.8a Effect of L_{cg} (m) on Longitudinal Stability Boundary

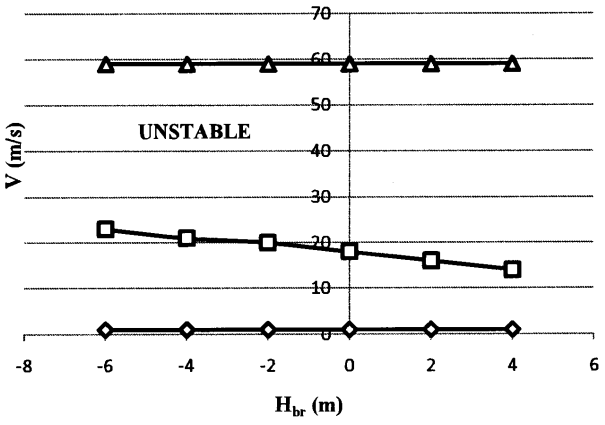

Fig.9b Effect of H_{br} (m) on Longitudinal Stability Boundary

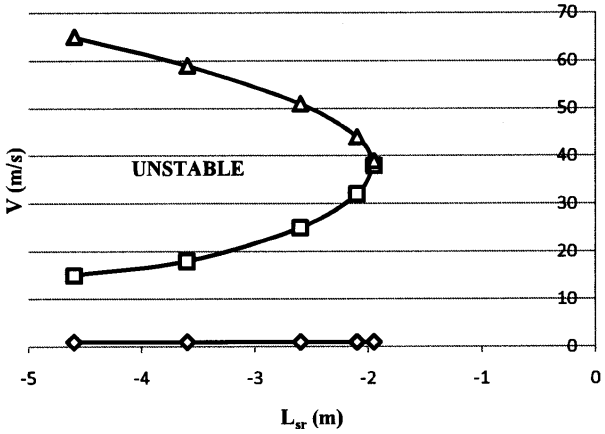

Fig.10a Effect of L_{sr} (m) on Longitudinal Stability Boundary

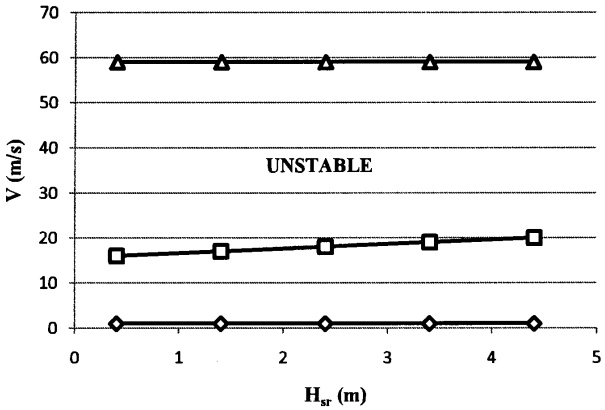

Fig.10b Effect of H_{sr} (m) on Longitudinal Stability Boundary

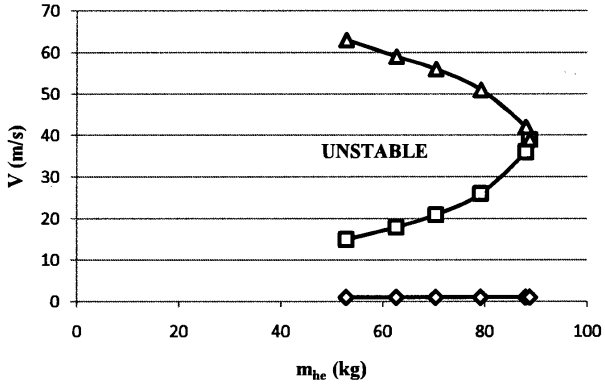

Fig.11 Effect of M_{he} (kg) on Longitudinal Stability Boundary

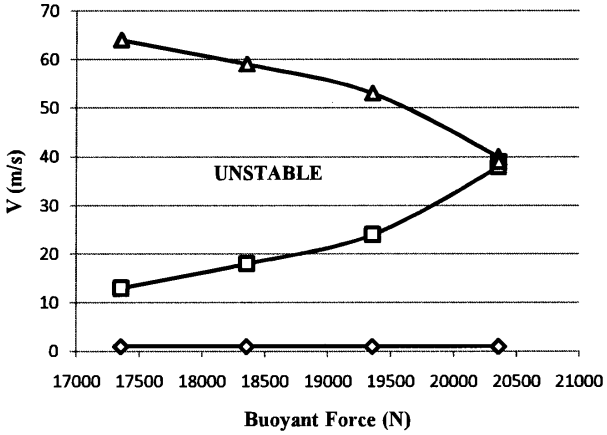

Fig.12 Effect of B (N) on Longitudinal Stability Boundary

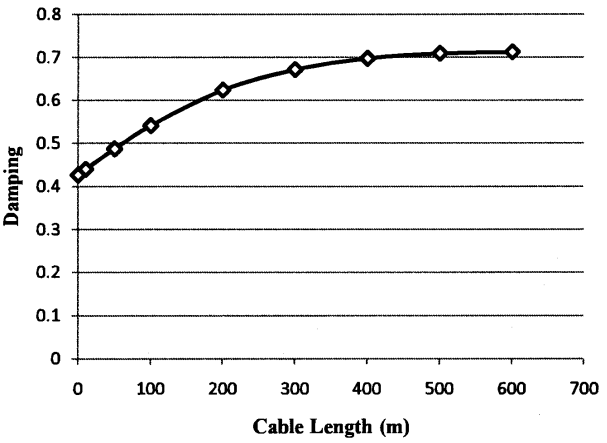

Fig.13 Effect of Cable Length (m) on Longitudinal Stability

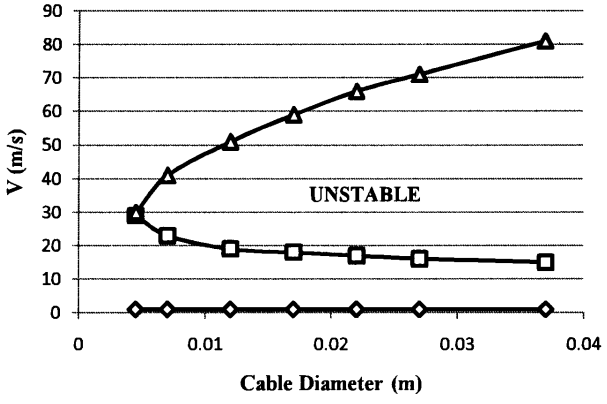

Fig.14 Effect of Cable Diameter [dc] (m) on Longitudinal Stability Boundary

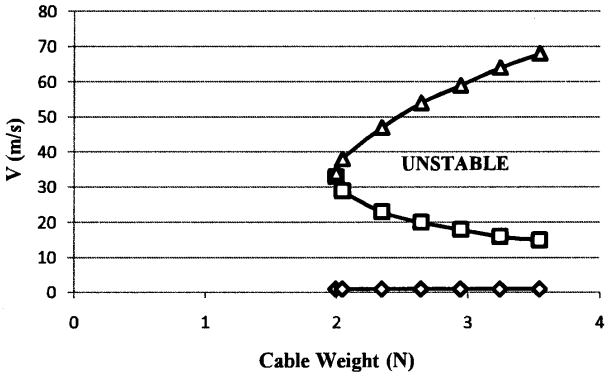

Fig.15 Effect of Cable Weight [w_c] (N) on Longitudinal Stability Boundary

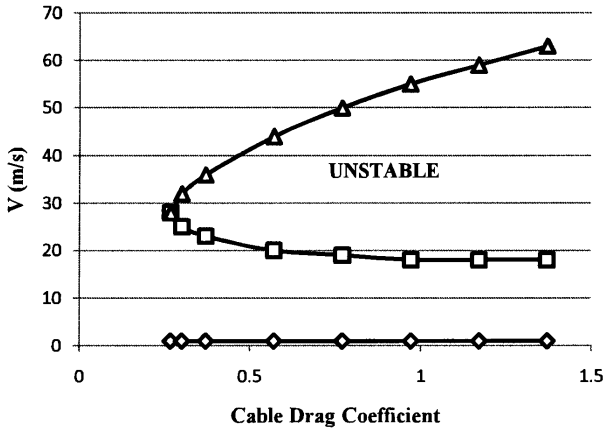

Fig.16 Effect of Cable Drag Coefficient (C_{Dc}) on Longitudinal Stability Boundary

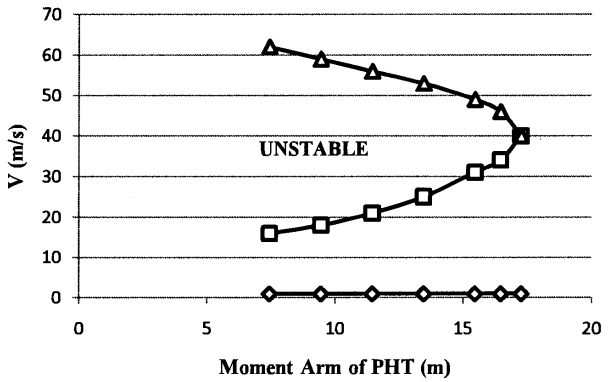

Fig.17 Effect of Moment Arm [PHT] (m) on Longitudinal Stability Boundary

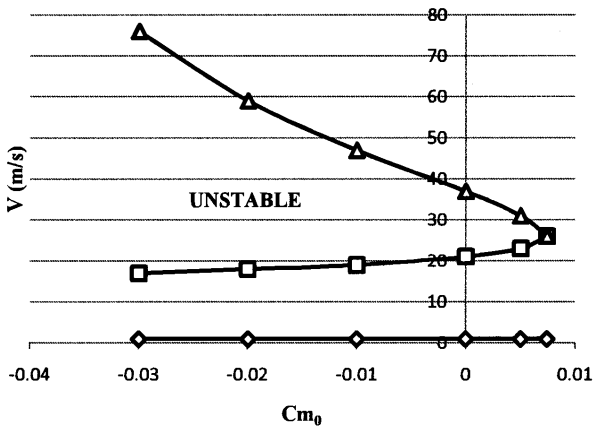

Fig.18 Effect of C_{mo} on Longitudinal Stability Boundary

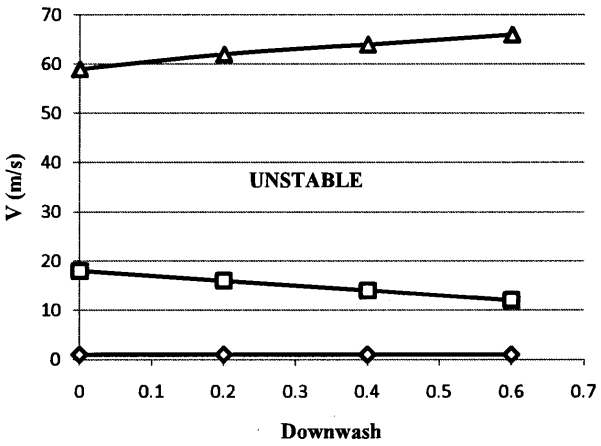

Fig.19 Effect of Downwash on Longitudinal Stability Boundary

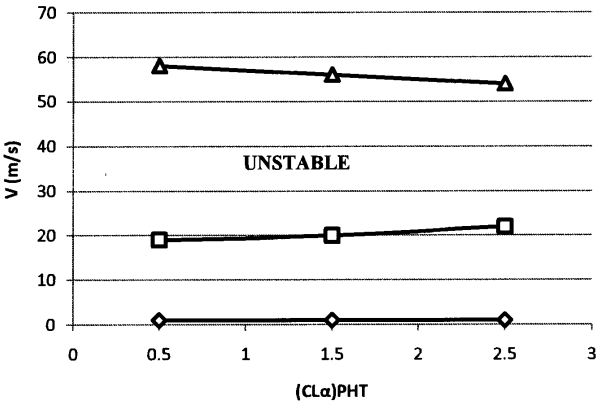

Fig.20 Effect of $(C_{L\alpha})_{PHT}$ on Longitudinal Stability Boundary